ELSEVIER

Journal of Alloys and Compounds 320 (2001) 18–23

Journal of ALLOYS AND COMPOUNDS

www.elsevier.com/locate/jallcom

Ferromagnetism in the strontium deficient $La_{0.67}Sr_{0.15}\square_{0.18}MnO_3$ perovskite manganite

L. Laroussi[a], A. Cheikhrouhou[a,*], J. Pierre[b]

[a]*Laboratoire de Physique des Matériaux, Faculté des Sciences de Sfax, B. P. 802, 3018 Sfax, Tunisia*
[b]*Laboratoire Louis NEEL, CNRS, B. P. 166X, 38042 Grenoble, France*

Received 22 December 2000; accepted 16 January 2001

Abstract

The structural, magnetic and magnetotransport properties of Sr deficient perovskite manganite oxide $La_{0.67}Sr_{0.15}\square_{0.18}MnO_3$ have been investigated. X-ray diffraction patterns have been indexed in the rhombohedral structure with *R*3*c* space group. Magnetic measurements showed that our sample exhibits a paramagnetic–ferromagnetic transition at $T_C = 360$ K, while electrical measurements show a maximum resistivity at $T_\rho = 210$ K. Strontium deficiency led to a strong decrease of the electrical transition temperature. At low temperature (20 K), a magnetic applied field of about 0.3 T induced a decrease of the resistivity of about 85%. At low temperature, our sample exhibited a magnetoresistance effect of about 30% under a magnetic applied field of about 4 T.

Keywords: Ferromagnetism; Strontium deficient perovskite manganite

1. Introduction

With the discovery of the very large negative magnetoresistance, great interest has been focused on the perovskite-type hole doped manganese oxides with the general formula $Ln_{1-x}M_xMnO_3$ where Ln is a trivalent rare-earth and M is a divalent alkali-earth [1–8]. These systems have been given much attention since they could possibly be used for sensor applications [9–11]. Different substitutions in these systems lead to different crystal structures, spin states and transport properties. The replacement of the trivalent element by a divalent or monovalent element produces mixed valence Mn^{3+}–Mn^{4+} ions to maintain charge neutrality and subsequently a modification occurs of both magnetic and transport properties. Such modifications can be understood on the basis of double-exchange interactions between the spins of the Mn^{3+} and Mn^{4+} ions [12,13]. However, recent studies have shown that the double exchange alone cannot explain the observed behaviors in these systems and suggested, that other effects ruled by average A-site cationic radius $\langle r_A \rangle$ [14–16], A-site cationic size mismatch [17,18], and oxygen deficiency [19–21] play a crucial role as to Mn valence, charge ordering or pinning, polaron effects and Jahn–Teller distortion [22].

Many studies are being carried out on the magnetic and magneto-transport properties of these materials. Effects of divalent alkaline-earth elements have been extensively studied [7–14]. These studies showed that the Curie temperature T_C and the magnetoresistance effects are optimized for a Mn^{4+} content of about 33%. However, only few studies have been carried out on deficiency effects in manganite systems [23–25]. Deficiencies in the A perovskite site lead to an increase in the Mn^{4+} content. In order to study the effects of vacancies in $La_{0.67}Sr_{0.33}MnO_3$, we investigate the structural, magnetic and electrical properties in the $La_{0.67}Sr_{0.15}\square_{018}$ MnO_3 deficient compound. In such sample, vacancy implies an increase of the Mn^{4+} content beyond 33% and also a change in the average ionic radius $\langle r_A \rangle$ of the A-site.

2. Experimental

A powder sample of $La_{0.67}Sr_{0.15}\square_{0.18}MnO_3$ was prepared by a conventional solid–solid reaction. The precursors La_2O_3, $SrCO_3$ and MnO_2 in the form of high-purity (>99%) powders were fired in air at 700°C for 10 h before being used. These materials were thoroughly mixed

*Corresponding author. Tel.: +216-4-274-390; fax: +216-4-274-437.
E-mail address: abdel.cheikhrouhou@fss.rnu.tn (A. Cheikhrouhou).

0925-8388/01/$ – see front matter
PII: S0925-8388(01)00944-6

in an agate mortar, in stoichiometric proportions and heated in air at 900°C for 48 h to achieve decarbonation. The resulting powder was then pressed into pellets form of about 1 mm thickness and fired at 1350°C for 36 h in air with several periods of grinding and sintering. Finally, the pellets were rapidly quenched to room temperature in water. This final step was carried out in order to retain the structure obtained at the sintered temperature 1350°C. In fact, studies on $Pr_{0.5}Sr_{0.5}MnO_3$ [26,27] showed that the quenching method has an important effect on the physical properties of these manganites.

Phase purity, homogeneity and lattice parameters were determined by X-ray powder diffraction using Guinier–Hagg cameras, with $CrK\alpha_1$ radiation, at room temperature. High-purity silicon powder was used as an internal standard. Unit cell parameters were obtained by least squares calculations.

Magnetization measurements versus temperature were recorded by a laboratory-made Faraday balance, whereas the susceptibility in 0.05 T was recorded with a vibrating sample magnetometer. Magnetization measurements versus magnetic applied field up to 8 T were recorded by an extraction magnetometer in the temperature range 20–430 K.

Electrical measurements as a function of the temperature and the magnetic applied field were performed on dense ceramic pellets by the conventional four-probe technique in the temperature range 20–300 K.

Table 1

	a_r (Å)	α_r°	V (Å^3)
$La_{0.67}Sr_{0.33}MnO_3$	5.469(0)	60.33	233.09
$La_{0.67}Sr_{0.15}\square_{0.18}MnO_3$	5.464(5)	60.25	232.11

3. Results and discussion

X-ray analysis shows that our sample exhibits practically identical X-ray powder patterns as stoichiometric $La_{0.67}Sr_{0.33}MnO_3$. We plot in Fig. 1 the X-ray diffraction (XRD) patterns at room temperature for both stoichiometric $La_{0.67}Sr_{0.33}MnO_3$ and Sr deficient $La_{0.67}Sr_{0.15}\square_{0.18}MnO_3$ samples. All the observed peaks are indexed in a perovskite structure with a distortion from the ideal cubic cell giving rhombohedral symmetry with $R\bar{3}c$ space group. We list in Table 1 the crystallographic data for both samples.

In order to check the oxygen stoichiometry, our sample was annealed at 800°C in air for 2 weeks. XRD patterns using a diffractometer ($\lambda = 1.54056$ Å) of both stoichiometric and deficient annealed samples (Fig. 2) showed no significant change in the structure. This result confirms that our deficient sample is not substoichiometric in oxygen.

We plot in Fig. 3 the magnetization evolution versus temperature of both stoichiometric and lacunar samples. Our sample exhibits a clear transition from a paramagnetic

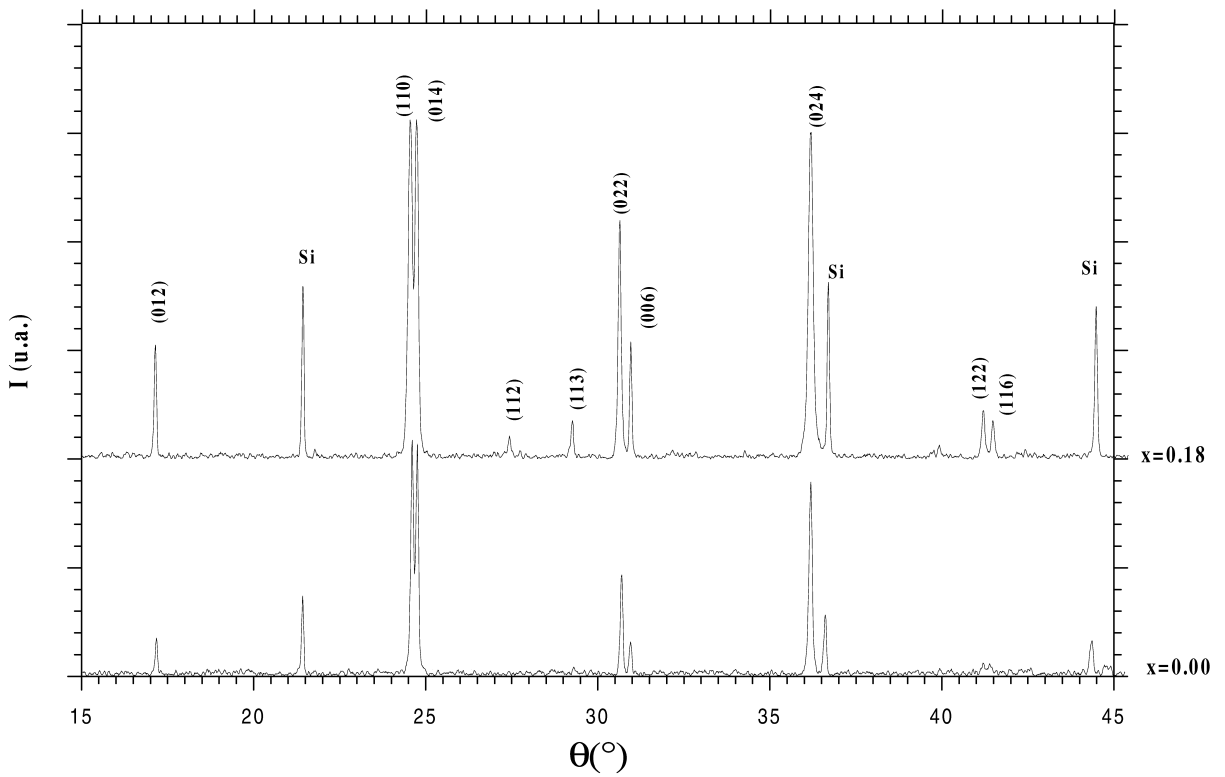

Fig. 1. X-ray diffraction patterns for both $La_{0.67}Sr_{0.15}\square_{0.18}MnO_3$ and $La_{0.67}Sr_{0.33}MnO_3$ samples.

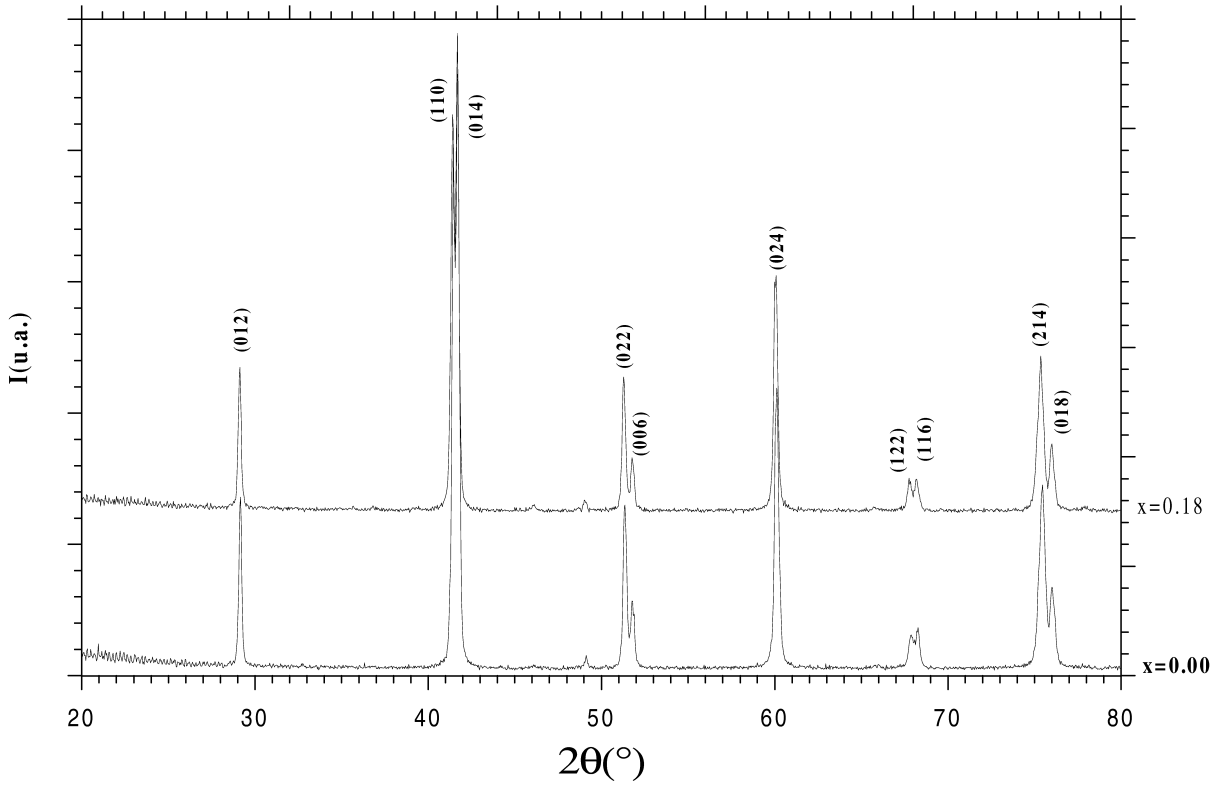

Fig. 2. X-ray diffraction patterns for both annealed $La_{0.67}Sr_{0.15}\square_{0.18}MnO_3$ and $La_{0.67}Sr_{0.33}MnO_3$ samples.

to a ferromagnetic state with decreasing temperature. The Curie temperature is found to be 360 K. Strontium deficiency induces a slight decrease in T_C, which is found to be 375 K for the stoichiometric sample.

Fig. 4 shows the magnetization evolution versus magnetic applied field up to 8 Tesla in the temperature range 20–430 K. The magnetization exhibits a sharp increase at very low magnetic applied field then saturates at 1T. This result confirms the ferromagnetic behavior below 360 K.

In order to determine with precision the Curie temperature, we have plotted in Fig. 5 Arrott curves (M^2 vs. H/M). The Curie temperature is found to be 360 K.

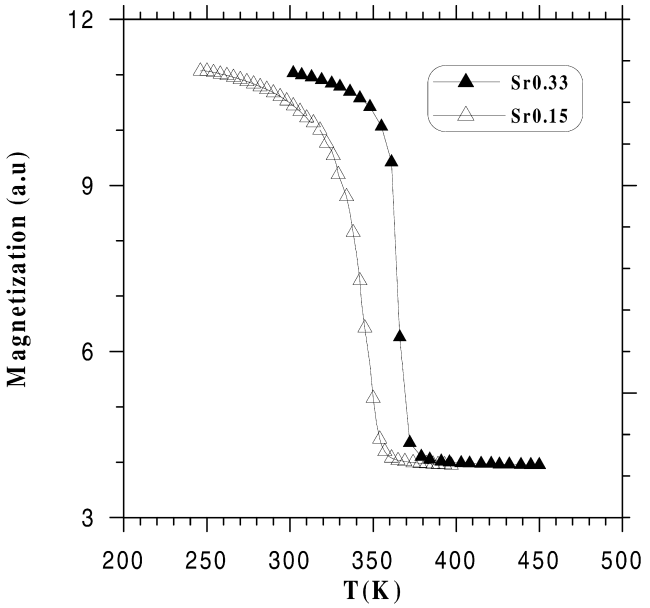

Fig. 3. Temperature dependence of the magnetization for $La_{0.67}Sr_{0.15}\square_{0.18}MnO_3$ and $La_{0.67}Sr_{0.33}MnO_3$ at $H=500$ Oe.

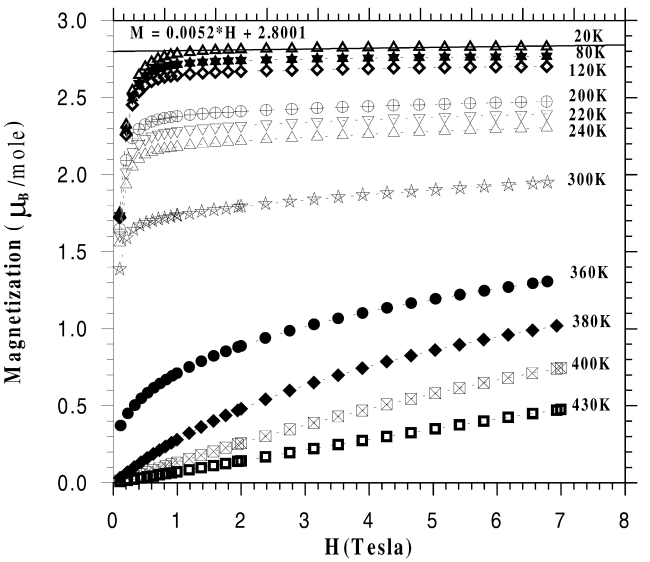

Fig. 4. Magnetization evolution versus applied magnetic field at several temperatures for $La_{0.67}Sr_{0.15}\square_{0.18}MnO_3$.

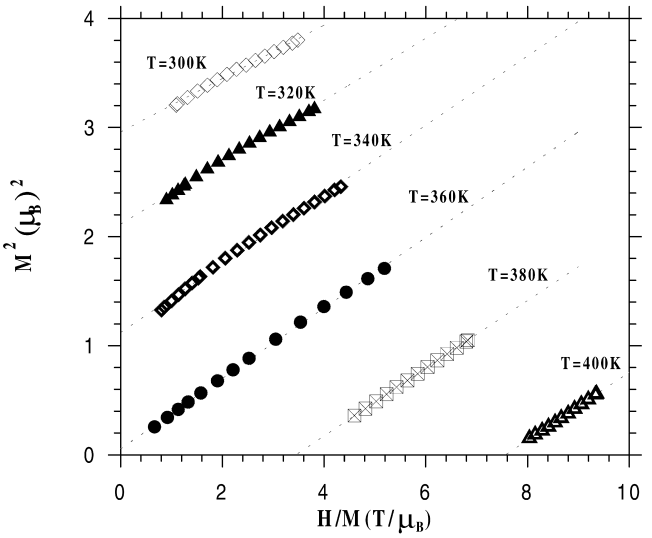

Fig. 5. Arrott curves $M^2(H/M)$ for $La_{0.67}Sr_{0.15}\square_{0.18}MnO_3$.

Fig. 6 shows the temperature dependence of the spontaneous magnetization (M_{sp}) and the inverse susceptibility (χ^{-1}) as function of temperature in our sample. The $M_{sp}(T)$ curve drops rapidly near $T_C = 360$ K showing a well defined Curie temperature. The magnitude of the spontaneous magnetization M_{sp} at 10 K is about 2.8 μ_B/Mn. The theoretical M_{sth} value for full alignment of the Mn ion spins (using $S = 4/2$ for Mn^{3+} and $S = 3/2$ for Mn^{4+}) is given by $M_{Sth} = 0.31 \times 4 + 0.69 \times 3 = 3.31$ μB/Mn. The experimental value is smaller than the calculated one which may indicate a canted spin state at low temperature. The angle ϕ between the average magnetic moments of the Mn cations in our sample can be obtained using the following equation

$$\cos\left(\frac{\phi}{2}\right) = \frac{M_{sp}}{M_{sth}} = \frac{2.8}{3.31} = 0.85$$

The angle ϕ is found to be 64°. The temperature dependence of the magnetic moment per mole $M_{sp}(T)$ can be described by the Brillouin–Weiss molecular field theory modeling the degree of spin collinearity.

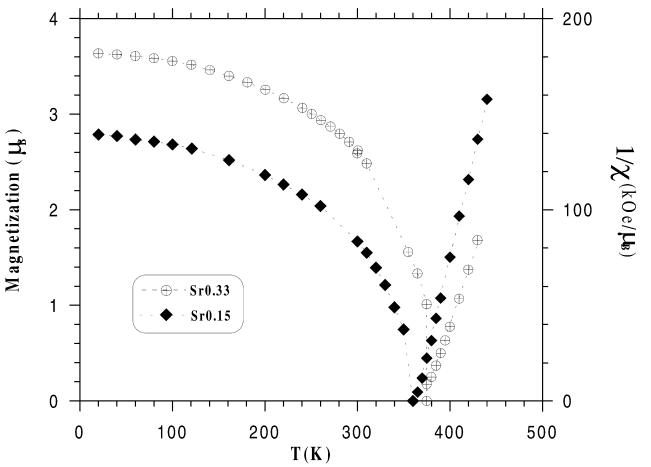

Fig. 6. Spontaneous magnetization and reciprocal susceptibility data versus temperature for $La_{0.67}Sr_{0.15}\square_{0.18}MnO_3$.

In the paramagnetic phase, the inverse of the susceptibility versus temperature exhibits the expected Curie–Weiss law $\chi = C/(T - \theta_p)$. From the linearity of the $\chi^{-1} - T$ curve, a net transition between the paramagnetic and the ferromagnetic states is confirmed corresponding to a paramagnetic Curie temperature $\theta_p = 363.8$ K. The obtained Curie constant C is 0.48 K·μ_B/kOe. For the stoichiometric sample $La_{0.67}Sr_{0.33}MnO_3$, θ_p and C are found to be 375 K and 0.65 K·μ_B/kOe, respectively. The strontium deficiency leads to a decrease in the T_C and θ_p values.

As a strontium vacancy induces an increase in the Mn^{4+} content, the T_C decrease observed in our sample can be explained by the increase of the Mn^{4+} concentration which leads to a decrease of the double exchange interactions. This result is in concordance with previous work on $La_{1-x}Sr_xMnO_3$ which shows a parabolic behavior of T_C versus Mn^{4+} content with a maximum obtained at about 33% [28]. However, the double exchange mechanism based on the Mn^{4+}:Mn^{3+} ratio alone cannot explain the observed behaviors in the diluted manganese oxides. The average A-site cationic radius $\langle r_A \rangle$ of the perovskite ABO_3 may play a crucial role. As a vacancy must have an average radius $\langle r_V \rangle \neq 0$, the T_C decrease due to the strontium deficiency in the lacunar $La_{0.67}Sr_{0.15}\square_{0.18}MnO_3$ sample can also be explained according to Hwang et al. [29] by a vacancy average radius $\langle r_V \rangle$ smaller than Sr^{2+} (1.31 Å). Such behavior has been observed in strontium deficient $Pr_{0.7}Sr_{0.3-x-x}MnO_3$ [25]. Finally the presence of vacancies traps the carriers and then lowers the double exchange interaction.

At zero applied field, resistivity measurements (Fig. 7) shows a semiconductor-metallic-like transition with decreasing temperature. The maximum of the resistivity is obtained at $T_\rho = 210$ K. This value is far below the Curie temperature, $T_C = 360$ K. The strontium deficiency leads to an increase of the resistivity values and a net decrease of the electrical transition temperature.

In the ferromagnetic range, the resistivity does not drop to very small values as in good metallic samples. In fact we deal with a granular material, thus there is a possibility that more or less insulating barriers develop at the grains boundaries. These barriers will limit the residual resistivity. This mechanism is well known in ceramics, in ferrite as well as in high T_C superconductors where insulating barriers cause the appearance of Josephson junctions below the transition temperature of the super-conducting grains [30].

As illustrated in Fig. 8, the effect of the magnetic field is to lower the value of the resistivity and to weaken its temperature dependence. Meanwhile the resistivity maximum becomes broader.

In the semiconductor-like phase, the conduction is

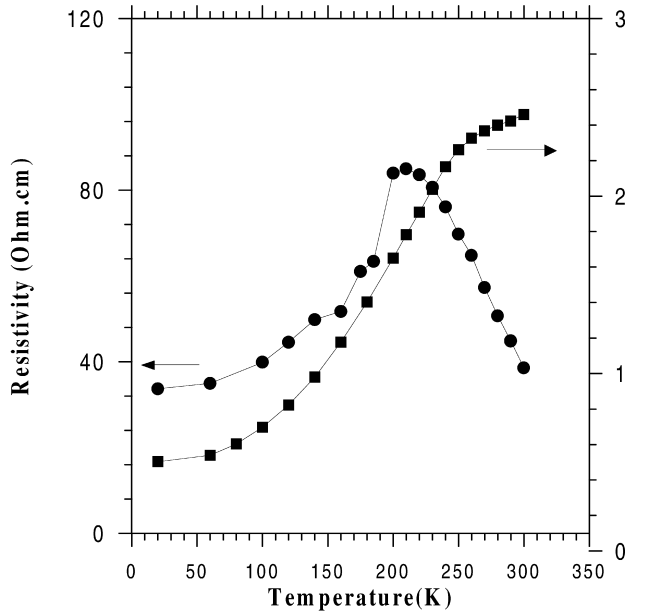

Fig. 7. Temperature dependence of the resistivity for both $La_{0.67}Sr_{0.15}\square_{0.18}MnO_3$ (●) and $La_{0.67}Sr_{0.33}MnO_3$ (■) samples.

thermally activated indicating polaron conduction. Above T_ρ, the zero field resistivity data fit quite well the formulae $\rho = \rho_0 \exp(E_a/kT)$ where E_a is the activation energy (Fig. 9). At zero applied field, the activated energy is found to be 0.35 eV. On applying a magnetic field H, the activation energy decreases with increasing H, decreasing from 0.35 eV at $H = 0$ to 0.31 eV at 4 T.

Defining the magnetoresistance MR as

$$\frac{\rho(H,T) - \rho(0,T)}{\rho(0,T)} \times 100$$

where $\rho(H, T)$ and $\rho(0,T)$ are the resistivities in an applied

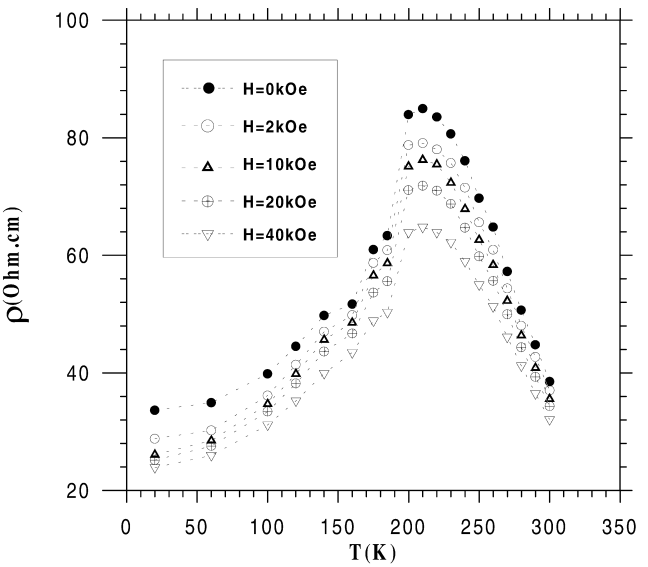

Fig. 8. Temperature dependence of the resistivity for $La_{0.67}Sr_{0.15}\square_{0.18}MnO_3$ at different applied magnetic fields.

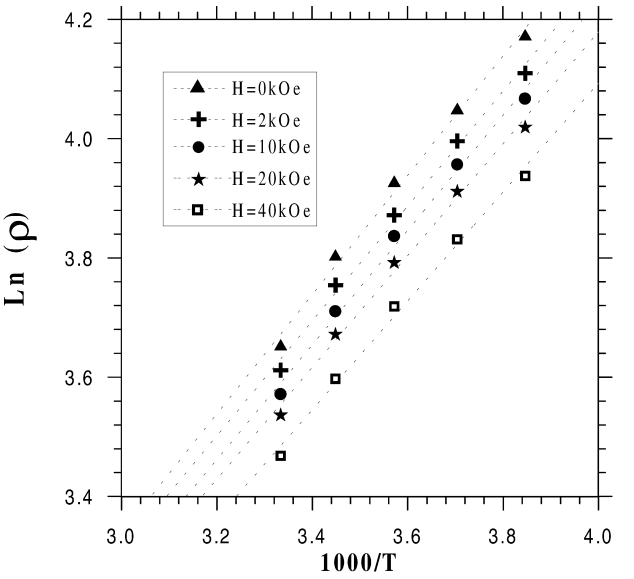

Fig. 9. Evolution of Ln (ρ) as function of $1/T$ for $La_{0.67}Sr_{0.15}\square_{0.18}MnO_3$.

magnetic field H and in zero field, respectively, we have plotted in Fig. 10 the magnetoresistance versus applied magnetic field for several temperatures. Below T_C, two regions in the field-dependence of the resistivity can be distinguished, which are seen better for the 20 K isotherm: an initial rapid drop in the region where the magnetization saturates, and a gentle decrease for larger fields. The first rapid drop of the resistivity that coincides with the saturation of the technical magnetization is due to the alignment of magnetization in neighboring grains, which occurs below 3 kOe in the ferromagnetic range. This MR is maximum at low temperature where $\rho(0,T)$ is minimum. The amplitude of this term is about 15% of the total resistivity at 20 K. The second regime situated above 3 kOe corresponds to a slower decrease of the resistivity, with a larger slope near the electrical transition temperature $T_\rho = 210$ K. This behavior is similar to the spin–disorder resistivity of ferromagnetic materials [31], but with a carrier density modified by the semiconducting–metal transition. These ferromagnetic grains being separated by high resistivity grain boundaries. Our sample exhibits a magnetoresistance behavior at low temperature of about 30% for a magnetic applied field of about 4 T.

4. Conclusion

We have investigated the structural, magnetic and magneto-transport properties of a deficient $La_{0.67}Sr_{0.15}\square_{0.18}MnO_3$ powder sample. Our sample crystallizes in the rhombohedral structure.

Magnetic measurements show a paramagnetic–ferromagnetic transition at $T_C = 360$ K. The strontium deficiency leads to a small decrease of T_C which can be

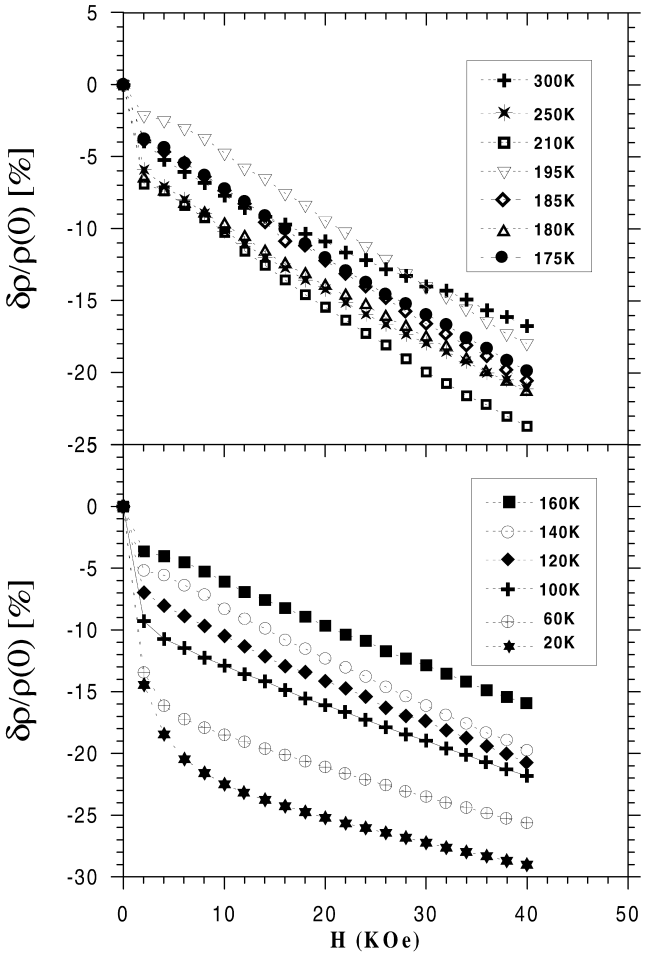

Fig. 10. Isotherms of MR for $La_{0.67}Sr_{0.15}\square_{0.18}MnO_3$ from 20 to300 K.

explained both by an increase of the Mn^{4+} content, a decrease of the ionic radius $\langle r_A \rangle$ of the A site and pinning of charge carriers by vacancies. Electrical investigations show a semiconducting–metallic like transition at 210 K related to the granular nature of the material. Our sample exhibits a magnetoresistance effect at low temperature of about 30% for a magnetic applied field of about 4 T.

References

[1] R. Von Helmolt, J. Wecker, B. Holzapfel, L. Schutz, K. Samwer, Phys. Rev. Lett. 71 (1993) 2331.
[2] R.D. Sanchez, J. Rivas, C.V. Vazquez, A.L. Quintela, M.T. Causa, M. Tovar, S. Oseroff, Appl. Phys. Lett. 68 (1996) 134.
[3] W. Zhang, I.W. Boyd, N.S. Cohen, Q.T. Quentin, A. Pankhaurst, Appl. Surf. Sci. 109 (1997) 350.
[4] F. Damay, C. Martin, M. Hervieu, A. Maignan, B. Raveau, G. André, F. Bourée, J. Magn. Magn. Mater. 184 (1998) 71.
[5] A. Peles, H.P. Kunkel, X.Z. Zhou, G. Williams, J. Phys.: Condens. Mat. 11 (1999) 8111.
[6] C. Martin, A. Maignan, M. Hervieu, B. Raveau, Phys. Rev. B 60 (1999) 12191.
[7] W. Boujelben, A. Cheikh-Rouhou, M. Ellouze, J.C. Joubert, Phys. Stat. Sol. (a) 177 (2000) 503.
[8] W. Boujelben, A. Cheikh-Rouhou, M. Ellouze, J.C. Joubert, Phase Transition 71 (2000) 127.
[9] J. Heremans, J. Phys. D 26 (1993) 1149.
[10] S. Jin, M. McCormack, T.H. Tiefel, R. Ramesh, J. Appl. Phys. 76 (1994) 6929.
[11] K. Derbyshire, E. Korezynski, Solid State Technol. (Sept.) (1995) 57.
[12] C. Zener, Phys. Rev. 81 (1951) 440.
[13] P.G. De Gennes, Phys. Rev. 118 (1960) 141.
[14] R. Mahesh, R. Mahendiran, A.K. Raychaudhuri, C.N.R. Rao, J. Solid State Chem. 114 (1995) 297.
[15] F. Damay, C. Martin, A. Martin, B. Raveau, J. Appl. Phys. 81 (1997) 1372.
[16] N. Abdelmoula, E. Dhahri, K. Guidara, J.C. Joubert, Phase Transitions 69 (1999) 215.
[17] L.M. Rodriguez-Martinez, J.P. Attfield, Phys. Rev. B 54 (1996) 15622.
[18] F. Damay, C. Martin, A. Maignan, B. Raveau, J. Appl. Phys. 82 (1997) 6181.
[19] A.K.M. Akther Hossain, L.F. Cohen, T. Kodenkandeth, J. MacManus-Driscoll, N. McNalford, J. Magn. Magn. Mater. 195 (1999) 31.
[20] I.O. Troyanchuk, S.V. Trukhanov, H. Szymezak, K. Baerner, J. Phys.: Condens. Mat. 12 (2000) L155.
[21] N. Abdelmoula, K. Guidara, A. Cheikh-Rouhou, E. Dhahri, J.C. Joubert, J. Solid State Chem. 151 (2000) 139.
[22] A.J. Millis, P.B. Littlewood, B.I. Shraiman, Phys. Rev. Lett. 74 (1995) 5144.
[23] L. Laroussi, J.C. Joubert, E. Dhahri, J. Pierre, A. Cheikh-Rouhou, Phase Transitions 70 (1999) 29.
[24] L. Laroussi, C. Boudaya, E. Dhahri, J.C. Joubert, A. Cheikh-Rouhou, Phase Transitions 68 (1999) 399.
[25] W. Boujelben, A. Cheikh-Rouhou, M. Ellouze, J.C. Joubert, Phys. Stat. Sol. (a) 181 (2000) 451.
[26] W. Boujelben, A. Cheikh-Rouhou, J. Pierre, J.C. Joubert, J. Alloys Comp. (2000) in press.
[27] W. Boujelben, A. Cheikh-Rouhou, J. Pierre, J.C. Joubert, J. Magn. Magn. Mat. (2001) in press.
[28] G.H. Jonker, Physica 22 (1956) 707.
[29] H.Y. Hwang, S.W. Cheong, P.G. Radaelli, M. Marezio, B. Batlogg, Phys. Rev. Lett. 75 (1995) 914.
[30] T. Grenet, Thesis, Joseph Fourrier University, Grenoble, 1992.
[31] P.G. de Gennes, J. Friedel, J. Phys. Chem. Solids 4 (1958) 71.